AGU PUBLICATIONS

Water Resources Research

RESEARCH ARTICLE
10.1002/2015WR018170

Key Points:
- We modeled seasonal and spatial dynamics of Lake Erie hypoxia
- We showed hypoxia starts nearshore and can persist after traditional monitoring programs end
- We recommend monitoring adjustments and explore impacts of different hypoxia definitions

Supporting Information:
- Supporting Information S1

Correspondence to:
S. A. Bocaniov,
bocaniov@umich.edu

Citation:
Bocaniov, S. A., and D. Scavia (2016), Temporal and spatial dynamics of large lake hypoxia: Integrating statistical and three-dimensional dynamic models to enhance lake management criteria, *Water Resour. Res.*, *52*, 4247–4263, doi:10.1002/2015WR018170.

Received 29 SEP 2015
Accepted 29 APR 2016
Accepted article online 3 MAY 2016
Published online 3 JUN 2016

Temporal and spatial dynamics of large lake hypoxia: Integrating statistical and three-dimensional dynamic models to enhance lake management criteria

Serghei A. Bocaniov[1] and Donald Scavia[1]

[1]Graham Sustainability Institute, University of Michigan, Ann Arbor, Michigan, USA

Abstract Hypoxia or low bottom water dissolved oxygen (DO) is a world-wide problem of management concern requiring an understanding and ability to monitor and predict its spatial and temporal dynamics. However, this is often made difficult in large lakes and coastal oceans because of limited spatial and temporal coverage of field observations. We used a calibrated and validated three-dimensional ecological model of Lake Erie to extend a statistical relationship between hypoxic extent and bottom water DO concentrations to explore implications of the broader temporal and spatial development and dissipation of hypoxia. We provide the first numerical demonstration that hypoxia initiates in the nearshore, not the deep portion of the basin, and that the threshold used to define hypoxia matters in both spatial and temporal dynamics and in its sensitivity to climate. We show that existing monitoring programs likely underestimate both maximum hypoxic extent and the importance of low oxygen in the nearshore, discuss implications for ecosystem and drinking water protection, and recommend how these results could be used to efficiently and economically extend monitoring programs.

1. Introduction

Monitoring, modeling, and predicting areas of low dissolved oxygen (DO) in the Great Lakes and coastal oceans is important because the number and size of these regions have increased [*Diaz*, 2001; *Diaz and Rosenberg*, 2008; *Vaquer-Sunyer and Duarte*, 2008] and more management programs are being put in place to reduce them [e.g., *Lake Erie*: *Hawley et al.*, 2006; *International Joint Commission* (*IJC*), 2012. *Gulf of Mexico*: *Mississippi River/Gulf of Mexico Watershed Nutrient Task Force* (*MR/GOM*), 2001, 2008. *Chesapeake Bay*: *U.S. Environmental Protection Agency*, 2010; *Chesapeake Bay Watershed Agreement*, 2014. *Baltic Sea*: *Helsinki Commission*, 2007. *Black Sea*: *International Commission for the Protection of the Danube River*, 2006, 2009]. However, developing and testing models to guide management action, as well as tracking progress associated with those actions, are often hampered by financially constrained monitoring programs. For example, the Gulf of Mexico's hypoxic zone, the largest in the United States and the world's second-largest coastal hypoxic zone [*Rabalais et al.*, 2007], is sampled systematically only once each year [*Rabalais et al.*, 2002; *Obenour et al.*, 2013]. Similarly, estimates of Lake Erie's hypoxic area are generally based on only one or two sampling cruises [*Zhou et al.*, 2013]. Recent advances in geostatistical modeling have improved those estimates. For example, *Obenour et al.* [2015] used auxiliary spatial information to improve hypoxic area estimates with quantified uncertainties for the Gulf of Mexico, and *Zhou et al.* [2013, 2014, 2015] and *Hansson et al.* [2011] used similar methods to provide best estimates and uncertainties for Lake Erie, Chesapeake Bay, and the Baltic Sea. However improved, these snapshots in time still constrain analysis of both long-term and seasonal trends in hypoxia development because they often miss critical periods of development and dissipation and likely underestimate the maximum extent, a typical endpoint of management concern [*MR/GOM*, 2001, 2008; *IJC*, 2012]. While additional monitoring can fill this gap, fiscal constraints have prohibited expanded monitoring as demonstrated by the lack of expanded monitoring efforts in many of these systems. Process-based, dynamic model interpolation of the sparse monitoring results can help provide important information. The aim of this study is to use a calibrated three-dimensional (3-D) hydrodynamic-ecological model to expand a relationship developed by *Zhou et al.* [2013] to estimate Lake Erie's hypoxic area (DO < 2 mg L^{-1}) as a function of average bottom water DO concentration from 10 central basin index stations. In doing so, we can explore the temporal and spatial development and dissipation of low-oxygen conditions in Lake Erie.

Lake Erie supports a multibillion dollar fishery and serves more than 11 million people in the United States and Canada. It experienced cultural eutrophication [*Beeton*, 1963], recovery in response to nutrient load reductions [*DePinto et al*., 1986], and a recent return to eutrophic conditions [*Burns et al*., 2005; *Bridgeman et al*., 2013; *Zhou et al*., 2013; *Michalak et al*., 2013; *Scavia et al*., 2014], with phosphorus (P) loading [*Dolan*, 1993; *Dolan and Chapra*, 2012] being the key driver of all three phases. This re-eutrophication has resulted in hypoxic extents comparable to levels of the past, with some reaching over 10,000 km^2 [*Zhou et al*., 2013], which in some years are comparable to or exceeding that of Gulf of Mexico [*Obenour et al*., 2013].

The most common index used in monitoring, modeling, forecasting, and tracking hypoxia is the maximum areal extent of DO concentrations below 2 mg L^{-1} [*Vaquer-Sunyer and Duarte*, 2008]. The work described herein is an effort to explore three aspects of that index: *thresholds, location, and dynamics*.

Thresholds - Though hypoxia can be defined as DO concentrations below 5–6 mg L^{-1} in freshwater and below 2–3 mg L^{-1} in marine and estuarine systems [*Farrell and Richards*, 2009], there is a broad range of definitions ranging from about 0.3–4 mg L^{-1} with an overall mean of 2.3 [*Vaquer-Sunyer and Duarte*, 2008] ($N = 49$ studies). The most commonly used index is 2 mg L^{-1} [e.g., *Committee on Environment and Natural Resources* (*CENR*), 2000; *Diaz*, 2001; *Zhou et al*., 2013, 2014, 2015; *Rucinski et al*., 2014], the point below which most aquatic organisms start to suffocate [*Diaz*, 2001], first suggested by *Renaud* [1986] based on the observations of fisheries collapse in Louisiana coastal waters. However, both higher and lower DO concentrations have negative ecosystem effects [*Vaquer-Sunyer and Duarte*, 2008]. For example (see supporting information Tables S1 and S2), DO < 1 mg L^{-1} causes substantial mortality in juvenile fish, DO < 3 mg L^{-1} forces Lake Erie fishes to migrate to areas with higher concentrations, DO < 4 mg L^{-1} is an acute mortality limit for invertebrates, and DO < 5 mg L^{-1} is a general suboptimal concentration for fish.

Location and Dynamics - The location and dynamics (timing, frequency, and duration) of hypoxia can affect the growth, distribution, and mortality of sessile and mobile aquatic organisms, including fishes of high economic importance [*Arend et al*., 2011]. Location is important because hypoxia can spatially overlap with otherwise high-quality habitats and/or ecologically important literal zones, limiting access to the areas of desirable thermal and light conditions, and/or habitats suitable for foraging, spawning, nursing, or protection from predation [*Roberts et al*., 2009; *Vanderploeg et al*., 2009; *Rao et al*., 2014; *Kraus et al*., 2015]. Timing is also important because hypoxia can occur during critical periods of spawning, egg development, and other recruitment stages [*Arend et al*., 2011].

Unlike its coastal marine counterparts, Lake Erie is also an important drinking water source. Water withdrawals from nearshore intakes can be as high as 68.9 km^3 yr^{-1} (2011 data) [*Great Lakes Commission*, 2013] representing 14.2% of the entire lake volume. Hypoxic and anoxic waters have low pH [e.g., *Howarth et al*., 2011] and elevated concentrations of manganese (Mn) [e.g., *Davison*, 1993] and other contaminants mobilized from the sediments. When such waters enter the distribution system, they compromise the water supply through enhanced pipeline and equipment corrosion; staining of fixtures, equipment, swimming pools, and laundry [*Sly et al*., 1990]; and often results in undesirable color of tap water. A strategy is emerging to use a buoy-based monitoring system near water intakes to alert shutdowns at the appearance of the advected anoxic water [*Ruberg et al*., 2008; *CENR*, 2010]. For example, the National Oceanic and Atmospheric Administration (NOAA) and the Cleveland Water Department deployed a buoy-based hypoxia early warning system that employs sensors near the water intakes to provide advance warning of hypoxia after three of four Cleveland water treatment plants were exposed to anoxic water in 2006, compromising the safety of the water supply for 1.5 million people [*Ruberg et al*., 2008]. While promising, the effectiveness of such strategies may be limited when more advance warning or prediction is needed to prepare for altered treatment strategies. Because water intakes are generally located in the nearshore zone, it could be important to better characterize the seasonal dynamics and interannual variability of nearshore hypoxia and anoxia.

2. Methods

2.1. Study Site Description

Lake Erie is located in North America (41°00′N–43°00′N latitude, 78°50′W–83°50′W longitude), and has three distinct basins, west, central, and east (Figure 1). Its central basin is approximately 63% of both total lake surface and volume [*Bolsenga and Herdendorf*, 1993]. Its surface area and volume are 16,138 km^2 and 305 km^3, and mean and maximum depths are 18.3 and 25.6 m. Depth-specific surface area and volume

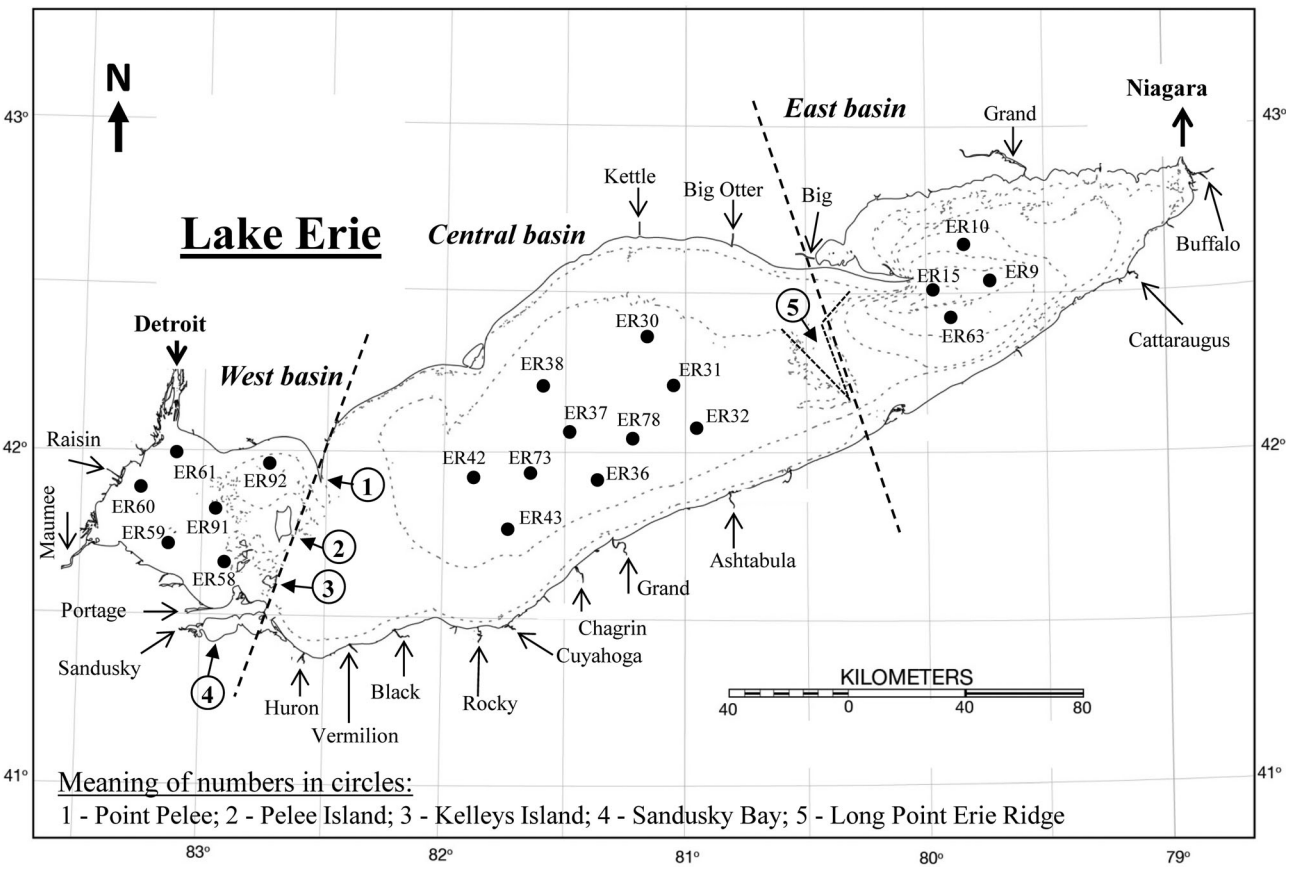

Figure 1. Map of Lake Erie with the locations of the USEPA stations and all included inflows and outflow (indicated by an arrow with the name of the corresponding river). Dotted lines represent 10 m contours.

show maxima at depths of 20 and 22 m. Using the 20 m contour as a boundary, the nearshore ($\leq$ 20 m) zone represent approximately 62.5% of central basin area and 53.4% of central basin volume.

2.2. Statistical Model

Zhou et al. [2013] provided a useful statistical relationship between hypoxic area and the average bottom water DO concentration from ten Lake Erie index stations (Table 1) visited routinely by the United States Environmentally Protection Agency (USEPA):

$$HE_2 = a \cdot e^{\left(\frac{-DO_m^2}{b}\right)} \quad (1)$$

where HE_2 is the area (10^3 km^2) with DO < 2 mg L^{-1}, DO_m is the mean DO concentration across the 10 USEPA index stations (Table 1), a and b equal 9.30 and 7.09, respectively [*Zhou et al*., 2013] ($R^2 = 0.97$, $N = 75$ cruises). We use the form of equation (1) throughout our analysis.

2.3. 3-D Modeling

Our ecological model is based on the dynamically coupled hydrodynamic-biogeochemical models, ELCOM-CAEDYM (ELCD). The Estuary and Lake Computer Model (ELCOM) is a three-dimensional hydrodynamic model that dynamically simulates water levels, thermal structure, temperature, velocity, and salinity distributions [*Hodges et al*., 2000; *Hodges and Dallimore*, 2006]. ELCOM is dynamically coupled with the Computational Aquatic Ecosystem Dynamics Model (CAEDYM) [*Hipsey*, 2008], a biogeochemical model capable of simulating of many biological, chemical, and sediment processes, as well as macrophytes, invasive species such as *Dreissenid* mussels [*Bocaniov et al*., 2014a] and several phytoplankton functional groups.

The ELCD model configuration was set similar to its previous applications to Lake Erie [e.g., *Bocaniov et al*., 2014a]. Lake Erie bathymetry was obtained from the NOAA National Geophysical Data Center. The physical

Table 1. The List of Index (Standard) Stations Located in the Central Basin of Lake Erie

Agency	Station Name	Latitude	Longitude	Depth (m)
USEPA (GLNPO)	ER30	42.4302	81.2050	19.6
	ER31	42.2535	81.1065	20.7
	ER32	42.0822	81.0118	21.5
	ER36	41.9350	81.4783	22.5
	ER37	42.1112	81.5750	23.5
	ER38	42.2817	81.6713	21.4
	ER42	41.9660	82.0420	21.5
	ER43	41.7892	81.9452	21.5
	ER73	41.9775	81.7570	23.5
	ER78	42.1165	81.2492	21.5
	Average depth:			*21.7*
EC	84	41.9361	81.6456	24.2
	945	42.4003	80.6411	20.6
	946	42.1667	80.6417	23.0
	949	42.2500	81.1081	22.2
	952	42.3583	81.4417	22.3
	953	42.2086	81.4419	23.2
	954	42.0250	81.4417	23.8
	961	41.9078	82.1833	20.5
	962	41.7167	82.1833	19.2
	Average depth:			*22.1*

Abbreviations: USEPA, United States Environmental Protection Agency; GLNPO, Great Lakes National Program Office; EC, Environment Canada.

domain was discretized into 2 × 2 km surface grids with 45 unevenly spaced vertical layers (0.5–5 m) to create the 3-D Cartesian mesh for the computational domain. Within the central basin, vertical layers were between 0.5 and 1 m thick. The time step was 300 s with output recorded every hour for water quality profiles and every 2 h for the bottom and surface layers. The model was run for 191 days from 21 April 2008 (DOY 112), the first date with sufficient initial conditions from the USEPA cruises, to 28 October 2008 (DOY 302), a date soon after the lake becomes well mixed and hypoxia dissipates.

In-lake initial conditions (water temperature, chemistry, and biology) were based on data from the USEPA Great Lakes National Program Office (GLNPO) monitoring program, derived from observations at twenty stations (Figure 1; east basin: ER9, ER10, ER15, ER63; central basin: ER30, ER31, ER32, ER36, ER37, ER38, ER42, ER43, ER73, ER78; west basin: ER58, ER59, ER60, ER61, ER91, ER92). These data were downloaded from the Great Lakes Environmental Database (GLENDA) available on the EPA Central Data Exchange (CDX) website [Web. 11 May 2015. <https://cdx.epa.gov/epa_home.asp>].

To account for spatial variability in meteorological drivers across such a large lake, meteorological forcing was represented by 13 different but approximately equal-sized zones (see supporting information Figure S1). Hourly meteorological observations of air temperature, wind speed, wind direction, relative humidity, solar radiation (shortwave), and cloud cover at 21 coastal stations and three in-lake buoys operated by the National Data Buoy Center and Environment Canada were corrected to account for the differences between overland and overlake conditions based on empirical relationships developed for Lake Erie [*Rodgers and Anderson*, 1961; *Schwab and Morton*, 1984; *Schertzer et al*., 1987], and then spatially interpolated to the 13 zones using a method of *Sambridge et al*. [1995]. Incoming longwave radiation was calculated first for the clear sky conditions [*Idso and Jackson*, 1969] and then adjusted for cloud cover [*Parkinson and Washington*, 1979].

One major outflow (Niagara River) and the 19 tributaries responsible for the majority of the discharge and nutrient loads to the lake (Table 2) were represented in the model (Figure 1). Four tributaries enter the west basin, eleven to the central basin, and four to the east basin. Concentrations of the water quality constituents, daily flow rates, and water temperatures for all tributaries were gathered from the Michigan Department of Environmental Quality (MDEQ), Heidelberg University Water Quality Laboratory, United States Geological Survey (USGS), Great Lakes Environmental Research Laboratory's (GLERL), STORET database of USEPA, Water Survey of Canada (Environment Canada), Provincial Water Quality Monitoring Network (PWQMN; Ontario, Canada), and Grand River Conservation Authorities (GRCA; Ontario, Canada).

Our main objective was to develop predictive equations for hypoxic extent that can be valid over the wide range of the meteorological conditions. To accomplish that, we used meteorological drivers representing the "warmest," "coldest," and "normal" years derived from the observed historical record of lake-wide surface water temperature. Daily lake-wide average surface water temperatures for 1995–2014, derived from the remote-sensing observations, were downloaded from Great Lakes Surface Environmental Analysis (GLSEA) website [Web. 11 May 2015. <http://coastwatch.glerl.noaa.gov/statistic/statistic.html>]. To determine baseline average conditions for this period, average daily mean lake surface temperatures were calculated for each day of the year by averaging all available data for each day over that 20 year period. The Root Mean Squared Error (RMSE) and Percent Bias (PBIAS) were calculated (supporting information Table S3) for

Table 2. Discharge and Phosphorus Load, Total (TP), and Soluble Reactive (SRP), in 2008 for the Tributaries Included in the Model (see also Figure 1)

		As % of Total Tributary Discharge or Nutrient Loads in 2008		
#	Tributary	Discharge	TP	SRP
West Basin				
1	Detroit	92.39	23.79	41.1
2	Raisin	0.33	2.50	1.9
3	Maumee	2.33	32.72	22.7
4	Portage	0.19	2.95	6.2
Central Basin				
5	Sandusky	0.44	9.8	6.1
6	Huron (Ohio)	0.14	1.7	1.3
7	Vermilion	0.10	1.3	1.3
8	Black	0.14	1.8	0.8
9	Rocky	0.12	1.1	1.1
10	Cuyahoga	0.41	4.1	3.1
11	Chagrin	0.15	1.3	1.9
12	Grand (Ohio)	0.31	1.6	0.6
13	Ashtabula	0.07	0.4	0.2
14	Big Otter	0.12	1.3	1.0
15	Kettle	0.05	0.7	0.8
East Basin				
16	Cattaraugus	0.34	2.5	1.2
17	Buffalo	0.38	0.7	0.6
18	Grand (Ontario)	1.16	6.1	5.4
19	Big	0.12	0.9	0.5
Total		*99.28*	*97.2*	*97.8*

each year relative to the baseline conditions. The RMSE was calculated separately for the entire year, as well as for the open water season (1 April to 30 October). The "normal" year was defined as the year with the smallest RMSE and PBIAS (2008; see below). PBIAS was used to determine both the warmest year (the largest absolute value of negative PBIAS; 2012, see below) and "coldest" year (the largest positive value of PBIAS; 1996, see below). Our baseline scenario used initial and boundary conditions from the "normal" meteorological year. "Warm" and "cool" scenarios used initial conditions, inflows/outflows, and nutrient load unchanged from the "normal" year, and meteorological conditions corresponding to those scenario years.

We use nutrient loads across all cases comparable to the current Lake Erie target load of 11,000 metric tonnes per annum (MTA) for all scenarios, determined by selecting loads from the year with the smallest absolute percent difference from the target load. This analysis identified both 1996 and 2008 but because 1996 lacked sufficient field observations for model validation, we used 2008.

In an earlier application to Lake Erie, ELCD was calibrated for 2002 for several of the most important water quality variables (major nutrients and their fractions; total phytoplankton biomass; light attenuation; suspended solids) and the seasonal succession of the major phytoplankton taxonomic groups [*Leon et al*., 2011]. In later applications for the same calibration year, it was extended to investigate mussels' role in the decline of Lake Erie's phytoplankton spring blooms [*Bocaniov et al*., 2014a]. The model was also previously validated for water temperature and thermal structure for 2008 [*Liu et al*., 2014]. Herein, we used the same calibration and extended that validation for DO and temperature at several spatial scales using a similar model configuration, but with higher resolution of meteorological input (13 versus 4 zones) and increased number of the tributaries (19 versus 11). In addition to the earlier validation work, the model's ability to reproduce the most dynamic part of the thermal structure (metalimnion) was analyzed quantitatively by comparing observed and modeled width and depth (thermocline position). The depth of the thermocline and the upper and lower boundaries of the metalimnion were determined with a fitting approach similar to that of *Read et al*. [2011] using the observed and modeled temperature profiles which were converted to the density profiles.

Data for validation came from water quality profiles measured in the central basin by USEPA during seven cruises in 2008 (20–22 April, 2–3 June; 24–25 June; 12–13 July; 10–11 August; 30–31 August; and 12–13 September). Validation data for the satellite-based lake-wide surface temperature observations in 2008 were obtained from the GLSEA website [Web. 12 May 2015. <http://coastwatch.glerl.noaa.gov/statistic/statistic.html>].

2.4. 3-D Model-Derived Relationships Between Low DO Areas and Bottom DO

To derive predictive equations for low DO areas (HE_i; HE is the hypoxic extent and *i* is the DO threshold concentration being evaluated), we ran the model for the "normal" year and calculated the daily areal extent of the hypoxic area based on 2 different thresholds (HE_2, DO < 2 mg L^{-1}; HE_1, DO < 1 mg L^{-1}) and the mean daily simulated bottom DO concentrations at the locations of the USEPA and the Environment Canada index central basin stations (Table 1). Using the curve-fitting function in R [*R Core Team*, 2014], we fit equation (1) to determine parameters *a* and *b* and their 95% confidence intervals (Table 3). We then used a

Table 3. Parameters (*a* and *b*) and Their 95% Confidence Intervals (2.5% and 97.5% Percentiles) for the Predictive Equations to Estimate the Hypoxic Extent Based on the Square of Mean Bottom DO Concentrations at the Locations of 10 USEPA Index Stations in Central Lake Erie[a]

Equation No	Hypoxic Extent (HE)	Zone	*a*			*b*			*N*	R^{2b}
			Mean	2.5%	97.5%	Mean	2.5%	97.5%		
	For EPA index stations (see Table 1)									
2	HE_1	Total	6.04	5.61	6.51	3.28	2.95	3.65	453	0.85
3	HE_2	Total	10.63	10.37	10.89	7.00	6.72	7.28	453	0.97
4	HE_3	Total	12.92	12.60	13.25	12.25	11.72	12.80	453	0.95
5	HE_4	Total	14.18	13.80	14.57	18.32	17.45	19.23	453	0.95
6	HE_1	Nearshore	1.93	1.81	2.06	7.12	6.38	7.95	447	0.79
7	HE_2	Nearshore	4.07	3.90	4.26	11.20	10.36	12.12	453	0.86
8	HE_3	Nearshore	5.72	5.50	5.94	16.26	15.17	17.42	453	0.87
9	HE_4	Nearshore	6.87	6.63	7.11	22.22	20.83	23.64	453	0.87
10	HE_1	Offshore	4.83	4.38	5.32	2.09	1.87	2.34	447	0.76
11	HE_2	Offshore	7.17	6.98	7.36	4.61	4.43	4.79	453	0.97
12	HE_3	Offshore	7.46	7.27	7.65	9.24	8.87	9.64	453	0.95
13	HE_4	Offshore	7.49	7.29	7.68	15.15	14.47	15.85	453	0.94
	For EC index stations (see Table 1)									
14	HE_1	Total	5.93	5.51	6.39	3.45	3.11	3.84	447	0.83
15	HE_2	Total	11.49	11.21	11.78	6.06	5.84	6.30	453	0.97
16	HE_3	Total	13.47	13.16	13.78	10.89	10.46	11.34	453	0.97
17	HE_4	Total	14.59	14.24	14.93	16.93	16.21	17.67	453	0.95
18	HE_1	Nearshore	2.16	2.03	2.31	5.83	5.30	6.44	447	0.83
19	HE_2	Nearshore	4.43	4.25	4.61	9.35	8.72	10.02	453	0.90
20	HE_3	Nearshore	5.98	5.77	6.19	14.37	13.48	15.29	453	0.90
21	HE_4	Nearshore	7.04	6.82	7.26	20.41	19.23	21.60	453	0.90
22	HE_1	Offshore	4.85	4.39	5.35	2.21	1.98	2.46	447	0.75
23	HE_2	Offshore	7.53	7.22	7.85	4.28	4.06	4.52	453	0.92
24	HE_3	Offshore	7.66	7.43	7.89	8.44	8.04	8.86	453	0.94
25	HE_4	Offshore	7.66	7.47	7.85	13.91	13.32	14.51	453	0.95

[a]All equations are in the form of equation (1) (see text).
[b]Abbreviations: R^2, coefficient of determination; *N*, the number of observations.

similar approach using a pooled data set consisting of the simulation results for the "normal," "cool," and "warm" years to derive the predictive equations for all four thresholds, HE_1, HE_2, HE_3 ($DO < 3$ mg L^{-1}), and HE_4 ($DO < 4$ mg L^{-1}).

2.5. Seasonal Trend in Stratification, Thermal Stability, and Potential for Mixing

To investigate the seasonal patterns in stratification and wind fields, we computed the basin-wide daily surface (depth ≤ 0.5 m) and bottom (depth > 20 m) temperatures (T_s and T_b) and wind speed. To quantify the importance of water column stability (thermal stratification), we calculated the Schmidt stability (*S*) [*Schmidt*, 1928; *Idso*, 1973], Brunt-Väisälä frequency (N^2) [*Väisälä*, 1925; *Brunt*, 1927], and wind stress (τ) [*Imberger*, 1985]. The time series of daily values of τ, *S*, and N^2 were computed for the conditions at station ER78 (Figure 1) using observed wind speed and simulated temperature profile assumed to be a good representation of the typical profile of stratification in the central basin.

3. Results

3.1. Model Validation

Our ELCD validation demonstrates the model's ability to adequately represent the 2008 field observations. The agreement between the observed and simulated temperatures was good, particularly for the lake wide surface temperature (Figures 2a, 2b; RMSE = 0.8°C, $N = 191$) and in the top 6 m of the surface mixed layer (Figure 2c; RMSE = 1.17°C, $N = 70$) which is good representative of the epilimnetic conditions in central Lake Erie [*Leon et al.*, 2011; *Bocaniov et al.*, 2014a]. Simulated bottom temperature at the 10 index USEPA stations that are representative of the central basin (Table 1) was also in good agreement with observations for all cruises (Figure 2d; RMSE = 1.99°C, $N = 70$) and the thermal structure of the central basin was well represented (Figures 3a–3n). The calculated RMSE between the measured and simulated profiles for stations ER31 (Figures 3a–3g) and ER78 (Figures 3h–3n), with comparisons made at 0.5 m depth increments, were 1.46°C ($N = 280$) and 1.95°C ($N = 280$), respectively. Simulated temperatures in the epilimnion and at

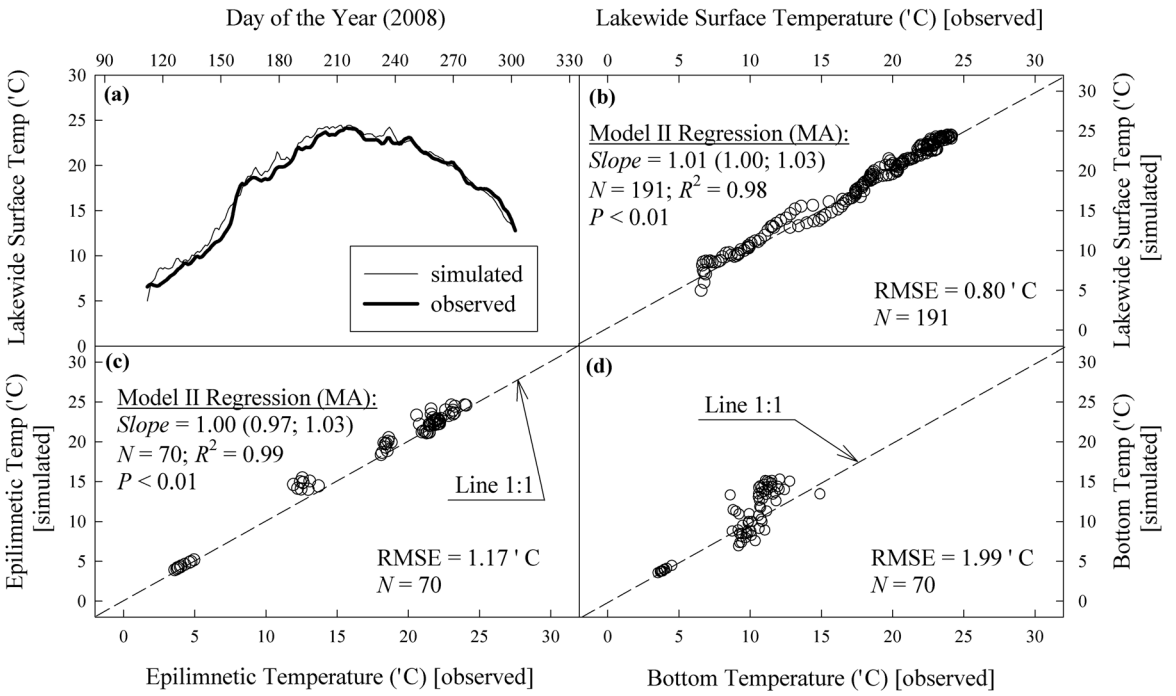

Figure 2. (a) Time series of the observed and simulated daily lake-wide surface temperatures; (b) plots of the observed versus simulated values of daily lake-wide temperatures, (c) temperatures averaged over the top six meters of the surface mixed layer, and (d) bottom temperatures.

the lower metalimnetic boundaries were in good agreement with the observed profiles (Figures 3a–3n). Simulated temperatures in the hypolimnion agreed within 1 or 2°C with the observed temperatures (Figures 3a–3n). The modeled thermocline position was reproduced well by model (supporting information Table S4). The width of the simulated metalimnion was wider than observed but the differences between the mean simulated and observed boundaries were smaller than the standard deviation of both observations and model for a given boundary. On average, the model had a small tendency to underestimate the depth of the upper metalimnetic boundary (PBIAS = 14.6%; $N = 50$) and overestimate the depth of the lower boundary (PBIAS = −8.5%; $N = 50$). Simulated DO concentrations were in good agreement with the observed values in the water column (Figures 3o–3r; RMSE = 1.22 mg L^{-1}, $N = 149$) and at the lake bottom (Figures 4a–4d; RMSE = 1.16 mg L^{-1}, $N = 70$). The regression analysis (major axis model II regression, Figure 4e) showed that the slope and the intercept were not significantly different from one and zero. The *t*-test also indicated no significant difference between observed and simulated mean bottom DO ($t = 1.7504$, $df = 69$, $P = 0.085$).

3.2. Lake Thermal Structure, Water Column Stability, and Potential for Wind-Induced Mixing

The seasonal dynamics of the surface temperatures (T_s) in the central basin followed the seasonal cycle of solar radiation (supporting information Figure S2a), increasing in spring and early summer, peaking from mid-July to early August, and declining afterward. Bottom temperature (T_b) steadily increased during the stratification period with a somewhat higher rate of increase near the end of the period (supporting information Figure S2a). The difference between T_s and T_b was small in April (22 April 2008: 1.7°C) but increased over the warming season, approached its maximum values in July (12.0°C), and declined to zero at lake overturn in early October (supporting information Figure S2a).

Overall, the temporal dynamic of winds over the lake surface also exhibited a clear seasonal pattern (supporting information Figure S2a). Winds were higher in the spring (April–May), weaker in early and mid-summer (June and July) and stronger in August and September, with the strongest winds in October. Winds were variable and episodic with weaker and stronger episodes with strong wind events typically occurring at 7–10 day intervals (supporting information Figure S2a). The computed values for Schmidt (*S*) and water column (N^2) stability showed seasonal patterns similar to observed T_s, mimicking the lake seasonal heating cycle (supporting information Figure S2). Water column stability and its resistance to wind mixing as judged

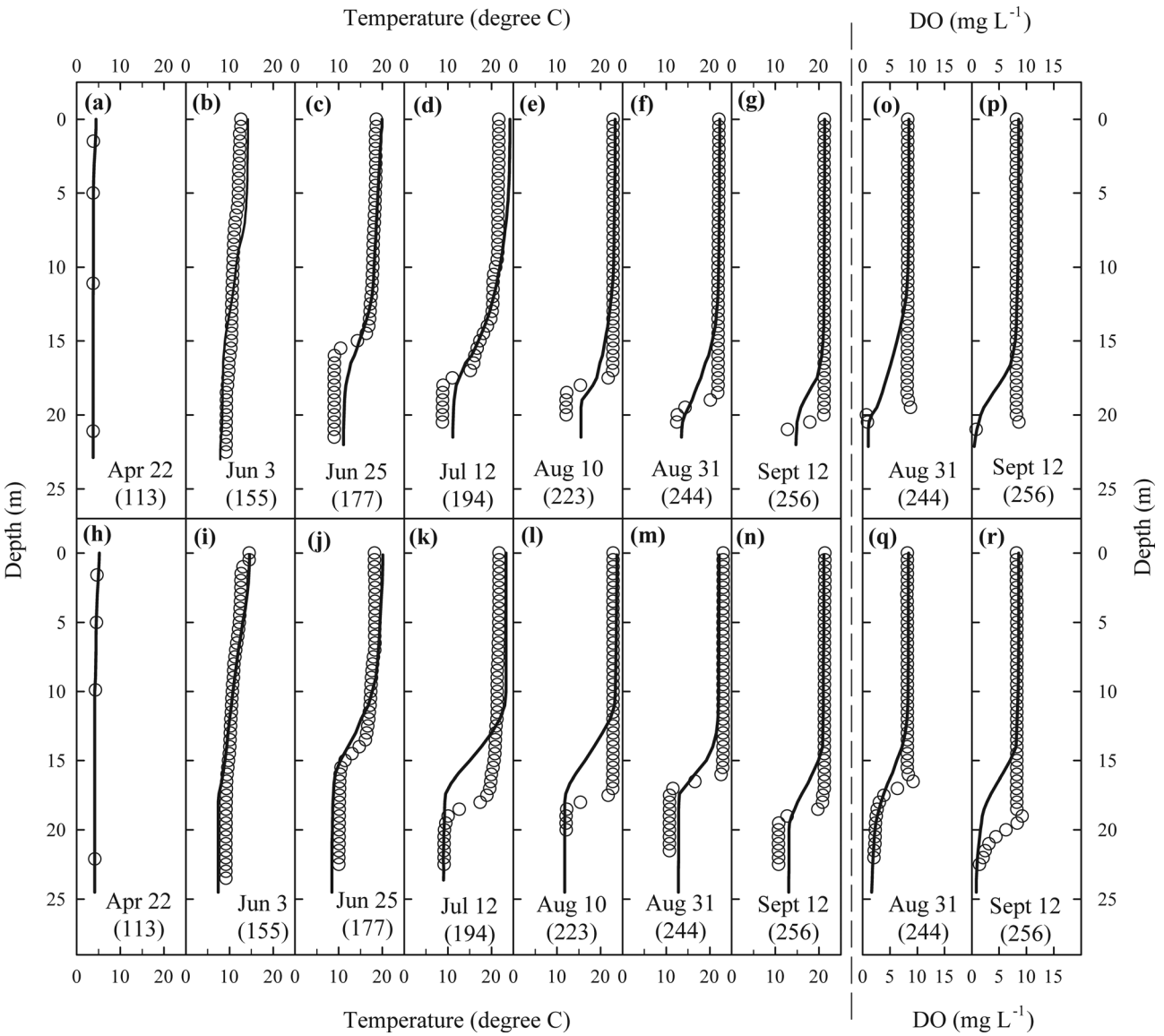

Figure 3. Comparison of the observed (open circles) and simulated (solid line) water column profiles at stations ER31 (a–g; o–p) and ER78 (h–n; q–r) for temperature (a–g; h–n) and dissolved oxygen (o–p; q–r).

by S and N^2 were low in spring but then increased rapidly from late May–June, reaching the seasonal maximum in July, and diminishing afterward. The strong wind events and corresponding high wind stress had noticeable effects on the lake thermal stability with increasing influences during the cooling phase and subsequent decline in the strength of thermal stability (August–September; supporting information Figure S2b).

3.3. Estimating Hypoxic Extent From Index Stations

There was good correspondence between simulated daily hypoxic extent (HE_2) for the baseline scenario and estimates using equation (1) [*Zhou et al.*, 2013] (herein referred to as the Zhou model) and mean simulated daily bottom DO concentrations (DO_m; mg L^{-1}) at the locations of ten USEPA index stations (Table 1; Figure 5a) until mid-September (Figures 5a and 5b). However, simulated mid-September to late October results often diverged from those predicted by the Zhou model (Figures 5a and 5c). Comparison of simulated hypoxic extent with estimates derived from the Zhou model and DO_m from simulated and field bottom DO concentrations at index stations showed good agreement overall, although the results derived from the Zhou model for early and mid-autumn again tend to underestimate the simulated results (Figure 5d; sim 1 versus sim 2).

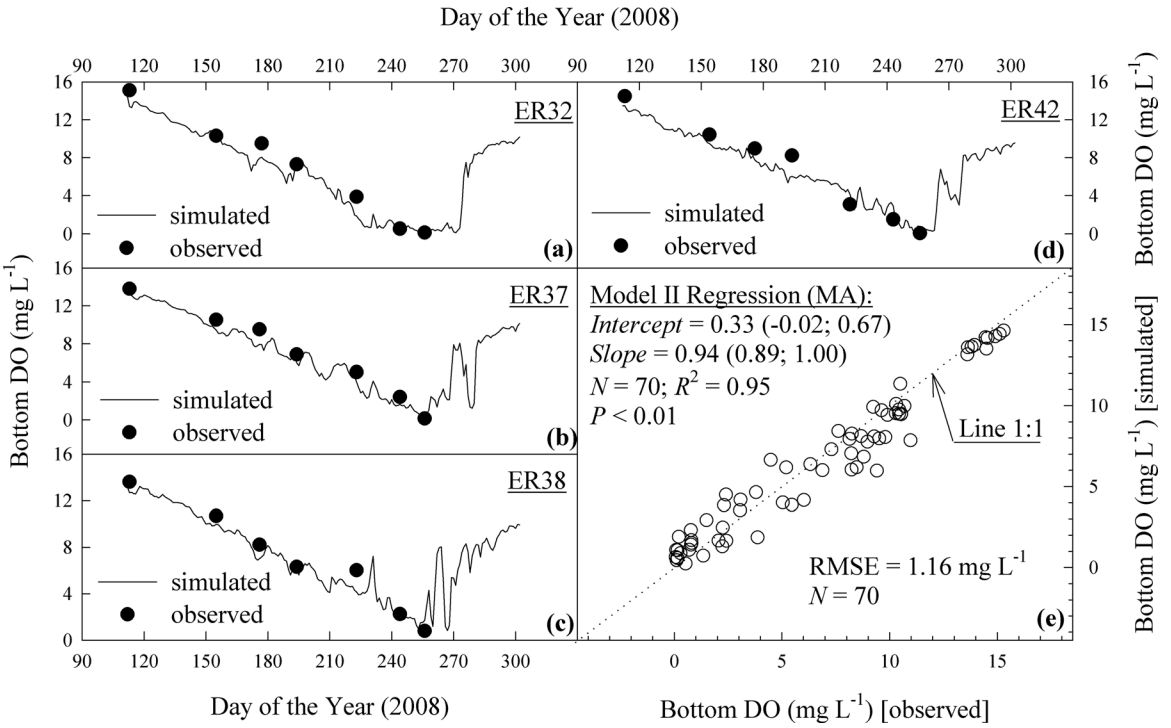

Figure 4. Observed (solid circles) and simulated (solid line) bottom dissolved oxygen (DO) at stations (a) ER32, (b) ER37, (c) ER38, and (d) ER42. (e) Simulated versus observed bottom DO for the seven USEPA cruises in 2008.

The comparison of simulated hypoxic extent HE_2 (Table 4) using equation (3) from Table 3 and observed field data for the GLNPO cruises from 2000 to 2012 with those reported by *Zhou et al*. [2013, 2015] was also very good (Figure 6a). A regression analysis (major axis model II regression, $N = 18$, $p < 0.01$) comparing the two estimates revealed that the slope was not significantly different from 1 (slope = 0.98 [95% CI: 0.89; 1.08]) and while the intercept was significantly different from zero (intercept = 0.83 [95% CI: 0.43; 1.19]), it was small, indicating a small systematic difference (0.83×10^3 km^2) between the two estimates. Nevertheless, all predicted values by equation (3) from Table 3 were within the range of the 95% C.I. reported by *Zhou et al*. [2013, 2015]. A one to one comparison of the results for selected cruises in 2003, 2005, and 2012 also revealed a reasonable match between the predictions of HE_2 using equation (3) and those calculated from the geostatistical method [*Zhou et al*., 2013, 2014] (Figure 6b).

3.4. Estimating Anoxic Area

Simulated daily HE_1 extent (DO < 1 mg L^{-1}; called anoxic extent herein) as a function of simulated mean daily DO concentrations (DO_m) at the USEPA index stations (Table 1) followed a pattern similar to that for HE_2 (Figure 7a) with additional outliers during a 6 day strong wind event (26–31 August 2008; supporting information Figure S2) that indicate a potentially higher sensitivity of HE_1 compared to HE_2 to wind events. When periods corresponding to the strong winds (26–31 August 2008) and early mid-autumn (14 September to 28 October 2008) were excluded, the relationship between HE_1 and DO_m was very strong ($R^2 = 0.97$; Figure 7b). The analysis also revealed a nonlinear relationship between HE_1 and HE_2 (Figure 7c). Comparison between the model simulations of the HE_1 with those predicted from the simulated daily DO_m using an equation shown in Figure 7b demonstrates a very good fit between two compared data sets (Figure 7d) and confidence in using the bottom DO concentrations at the ten USEPA index stations in the central basin to estimate the spatial extent of both HE_1 and HE_2.

3.5. Estimating HE_1, HE_2, HE_3, and HE_4 for a Wider Range of Meteorological Conditions

Using the approach outlined above, we developed predictive equations for simulated HE_1, HE_2, HE_3, and HE_4 as a function of mean bottom DO concentrations observed at either the USEPA index stations or Environment Canada index stations (Table 1) for the pooled data set representing "normal", "cool", and "warm" years. The resulting equations have high R^2 values (Table 3), indicating good fit overall. Using equations (2)–(5)

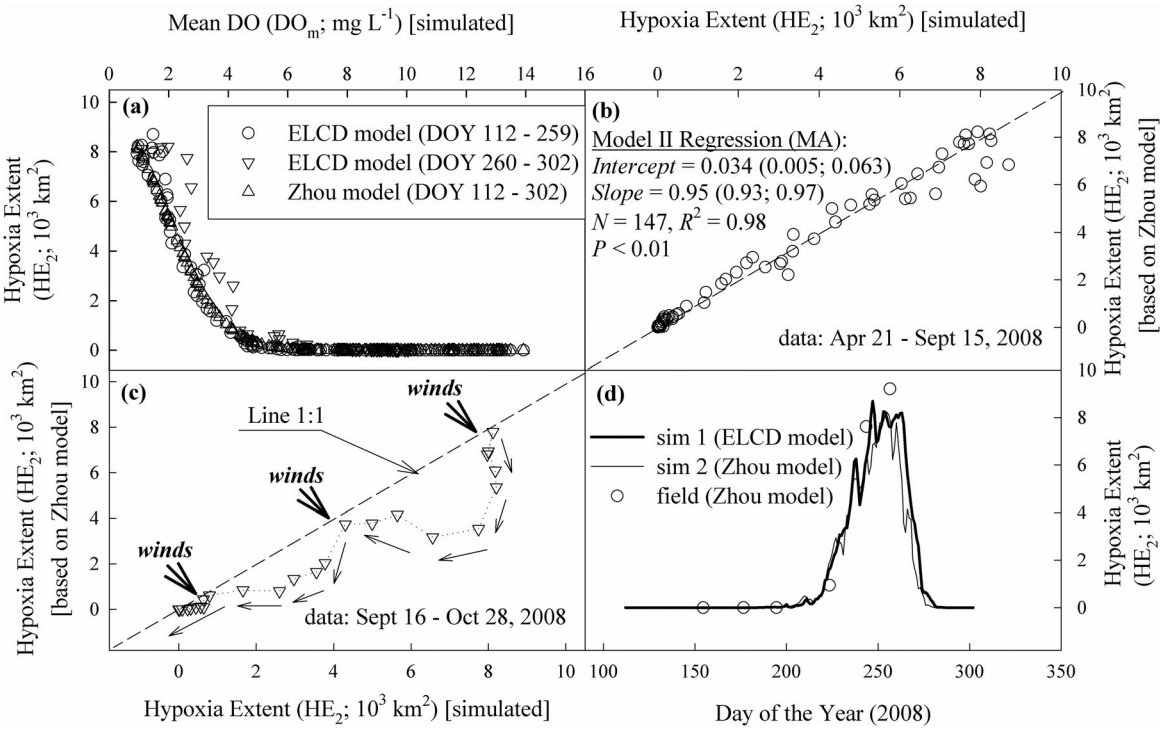

Figure 5. Plot of daily hypoxic extents HE_2 simulated by the 3-D model and those predicted from the Zhou model versus the average simulated daily bottom DO at 10 USEPA index stations in central Lake Erie (DO_m) for 2008 for the period from (a) 21 April to 30 October, (b) from 21 April to 15 September, and (c) from 16 September to 28 October. The thin arrows on Figure 5c show the progression of time, while the thicker arrows with the label "winds" indicate the times of the occurrences of the strong wind events (see also supporting information Figure S2 for the strong wind events). (d) Time series plots of HE_2 of the simulated results with 3-D model (thick solid line) and predicted by the Zhou model based on the average simulated daily bottom DO at ten USEPA index stations (thin solid line) and field observations (open circles).

(Table 3) we calculated the HE_1, HE_2, HE_3, and HE_4 using average measured concentrations from the August USEPA cruises in 2000 through 2014 (Figure 8). Results show that areal extents for lower DO thresholds have larger interannual variability. For example, the average absolute percent difference between annual values and their overall (interannual) mean were 119%, 78%, 57%, and 37% for HE_1, HE_2, HE_3, and HE_4, respectively.

3.6. Spatial Seasonal Dynamics of Total, Nearshore, and Offshore Hypoxia

Simulated seasonal dynamics of HE_1 and HE_2 are compared for the entire central basin, as well as separately for the nearshore and offshore zones, for "normal" (Figures 9a and 9b), "cool" (Figures 9c and 9d), and "warm" (Figures 9e and 9f) years. As expected, whole-basin HE_2 was larger during the "warm" year and smaller during the "cool" year compared to the "normal" year. Anoxia (HE_1) was also the smallest during the "cool" year but somewhat larger in the "normal" year compared to the "warm" year (Figures 9a, 9c, and 9e). Results also show that HE_2 starts first in the nearshore and then extends further to the offshore (Figures 9b, 9d, and 9f). A similar pattern was observed with HE_1 (Figures 9a, 9c, and 9e) although it was not as clear for the "normal" year (Figure 9a). Nearshore HE_1 and HE_2 were nearly the same offshore in "cool" and "warm" years, but smaller in the "normal" year (Figures 9a–9f).

Comparing seasonal dynamics of HE_1, HE_2, HE_3, and HE_4 for "normal" (Figure 10a), "cool" (Figure 10b) and "warm" (Figure 10c) years showed that HE_3 and HE_4 appear less affected by the warm and cool extremes from the historical record, suggesting that their timing and extent are more predictable under future climates (maximum extent: $HE_3 = 10–12 \times 10^3$, and $HE_4 = 12–13 \times 10^3$ km^2) compared to the lower thresholds. Also worth noting is that HE_3 and HE_4 can occupy the large proportions of the central basin for extended time periods.

4. Discussion

4.1. Model Validation

We demonstrate the ability of ELCD, previously calibrated for 2002, to reproduce field observations from 2008 of average lake-wide surface temperatures (Figures 2a and 2b), epilimnetic temperatures averaged

Table 4. Mean and 95% Confidence Intervals (2.5% and 97.5% Percentiles) in Brackets of Estimated Hypoxic Extent Based on Bottom Measurements of DO at 10 Index Stations in the Central Lake Erie From Summer GLNPO Cruises for 2000–2014 Using Formulas Derived From Three-Dimensional Hydrodynamic and Water Quality Model of Lake Erie (see Table 3)

			Hypoxic Extent (HE; 10^3 km^2)			
Year	Month	Date	HE_1	HE_2	HE_3	HE_4
2000	8	3–4	2.50	7.03	10.33	12.11
			(2.32–2.95)	(6.86–7.32)	(10.09–10.68)	(11.79–12.54)
2001	8	5–6	0.62	3.66	6.80	9.44
			(0.58–0.84)	(3.57–3.91)	(6.64–7.14)	(9.19–9.89)
2002	8	6–7	0.03	0.88	2.71	5.46
			(0.03–0.05)	(0.85–0.99)	(2.65–2.95)	(5.32–5.87)
2003	8	8	0.15	1.90	4.46	7.35
			(0.14–0.24)	(1.86–2.08)	(4.36–4.76)	(7.15–7.79)
2004	8	6	No Anoxia	0.36	1.54	3.90
				(0.35–0.43)	(1.51–1.71)	(3.80–4.27)
2005	8	9–10	0.02	0.72	2.39	5.07
			(0.02–0.04)	(0.70–0.82)	(2.34–2.62)	(4.93–5.47)
2006	8	10–12	0.51	3.33	6.39	9.10
			(0.47–0.70)	(3.25–3.57)	(6.24–6.73)	(8.86–9.55)
2007	8	8	0.09	1.52	3.86	6.74
			(0.09–0.16)	(1.40–1.68)	(3.77–4.15)	(6.56–7.18)
2008	8	9-10	0.03	0.93	2.81	5.59
			(0.03–0.06)	(0.91–1.05)	(2.75–3.06)	(5.44–6.00)
2009	8	18–19	No data	No data	No data	No data
2010	8	9–10	0.46	3.20	6.22	8.96
			(0.43–0.65)	(3.12–3.43)	(6.08–6.56)	(8.72–9.41)
2011	8	10	0.02	0.77	2.49	5.19
			(0.02–0.04)	(0.75–0.87)	(2.43–2.72)	(5.05–5.60)
2012	8	10	3.21	7.90	11.14	12.66
			(2.98–3.69)	(7.71–8.19)	(10.88–11.48)	(12.32–13.08)
2013	8	10	2.45	6.97	10.27	12.06
			(2.27–2.89)	(6.79–7.25)	(10.03–10.62)	(11.74–12.49)
2014	8	14–15	No anoxia	0.02	0.25	1.33
				(0.02–0.03)	(0.25–0.30)	(1.30–1.53)

over the top 6 m (Figure 2c), bottom temperatures (Figure 2d), thermal structure (Figures 3a–3n; supporting information Table S4), and both surface and bottom DO concentrations (Figures 3o–3r and 4). The calculated RMSE were similar and within the range of those reported in other three-dimensional modeling studies [*Huang et al*., 2010; *Leon et al*., 2011; *Beletsky et al*., 2013; *Liu et al*., 2014; *Bocaniov et al*., 2014a, 2014b].

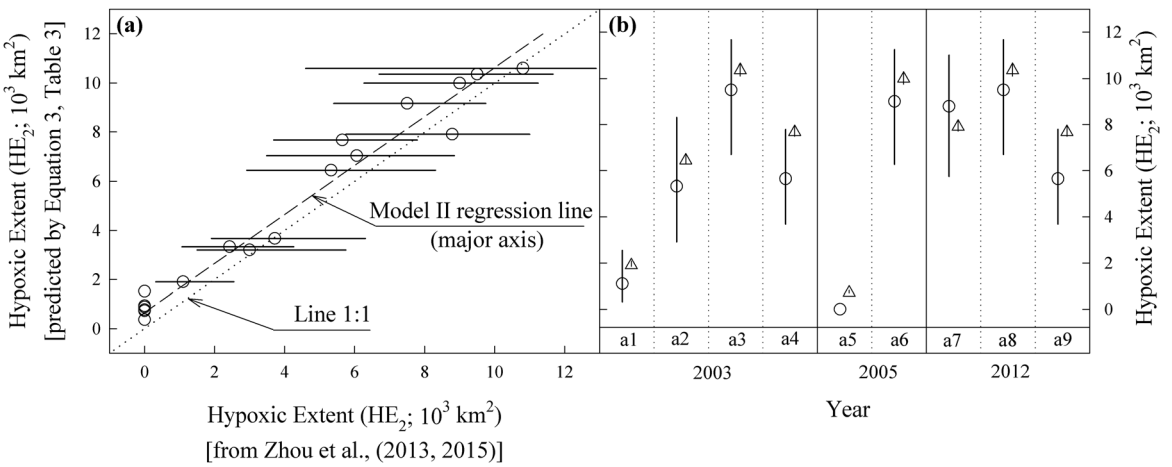

Figure 6. (a) Comparison of the hypoxic extents HE_2 in the central basin between those predicted by equation (3) (Table 3) from the field bottom DO observations and those reported in *Zhou et al*. [2013, 2015] for the late summer (August) GLNPO cruises from 2000 to 2012 inclusive including the data shown in right plot. Horizontal thin solid lines indicate the 95% confidence intervals in *Zhou's et al*. [2013, 2015] results. (b) Hypoxic extents HE_2 for some selected years, 2003, 2005, and 2012, with the following dates: 8 August and 19–20 August (a1, a2), 2–3 September and 15–16 September (a3, a4); 6 August and 15–16 September (a5, a6); 10–11 August, 30–31 August, and 10–11 September (a7, a8, a9). The median values from *Zhou et al*. [2013, 2015] are shown by the open circles; while open triangles indicate the mean values calculated using equation (3) (Table 3) from the field bottom DO observations. Vertical thin solid lines indicate the 95% confidence intervals (2.5% and 97.5% percentiles).

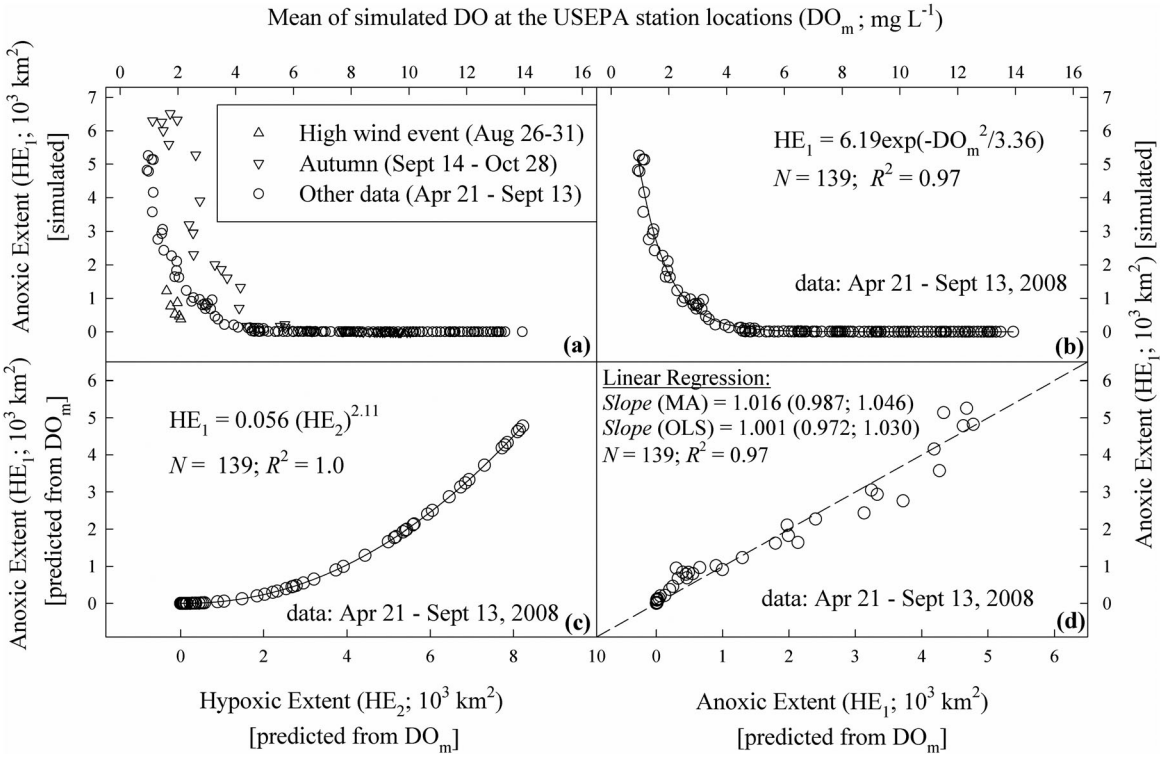

Figure 7. Plot of daily (anoxic) extent HE_1 versus average simulated daily bottom DO at 10 USEPA index stations in the central Lake Erie (DO_m) for the entire simulation period in (a) 2008 and (b) for the period from 21 April to 13 September 2008. (c) Plot of anoxic extents HE_1 predicted by equation for HE_1 shown in Figure 7b and based on simulated DO_m and hypoxic extents HE_2 predicted by Zhou model [*Zhou at al.*, 2013] for the same DO_m. (d) Plot of anoxic extents HE_1 simulated by 3-D model vs those HE_1 predicted by Zhou model and based on simulated DO_m.

Accurately modeling Lake Erie's metalimnion dynamics is difficult due to numerical diffusion, a very sharp metalimnion [*Schertzer et al.*, 1987], and its highly dynamic nature and sensitivity to wind fields [*Beletsky et al.*, 2013]. In addition, when present, it is the most dynamic part of the thermal structure so that small mismatches in time and space between modeled and observed phases appear as large errors. We are not aware of any other modeling studies of Lake Erie that quantitatively characterized the vertical structure of the modeled metalimnion (thermocline position, and upper and lower boundaries). Our results are a first attempt to do that, and we showed good comparisons to the thermocline depth (supporting information Table S4) with upper and lower boundaries of the metalimnion represented reasonably well compared to the other Lake Erie studies [*Beletsky et al.*, 2013; *Liu et al.*, 2014]. The more diffused nature of the modeled metalimnion in our study does not affect our results because the surface and bottom temperatures, the thermocline position (depth of the maximum change in density), and near-bottom oxygen dynamics are all well reproduced by model.

4.2. Seasonal Dynamics

Geostatistical modeling have improved estimates of the spatial extent of hypoxia in Lake Erie [*Zhou et al.*, 2013, 2015]; however, even these improved estimates are limited to relatively few snapshots in time constrained by the observation set. As a result, the regression model derived from those geostatistical estimates is limited to observations collected during basin-wide cruises through August or the first half of September (see supporting information Table S1 in *Zhou et al.* [2013]), a period when stratification is still strong (e.g., supporting information Figures S2b) and hypoxic area may still be growing (Figure 9; see also supporting information Figures S2). For example, the maximum possible hypoxic area derived from Zhou model is 9300 km^2, whereas hypoxic area has been reported to be as large as 11,000 km^2 [*Beeton*, 1963] (supporting information Table S1 in *Zhou et al.* [2013]). This has important implications because several recent modeling efforts have used this relationship to convert zero, 1, and 2-dimensional model outputs to hypoxic area [*Scavia and DePinto*, 2015] and the upper limit of the regression model may underestimate the

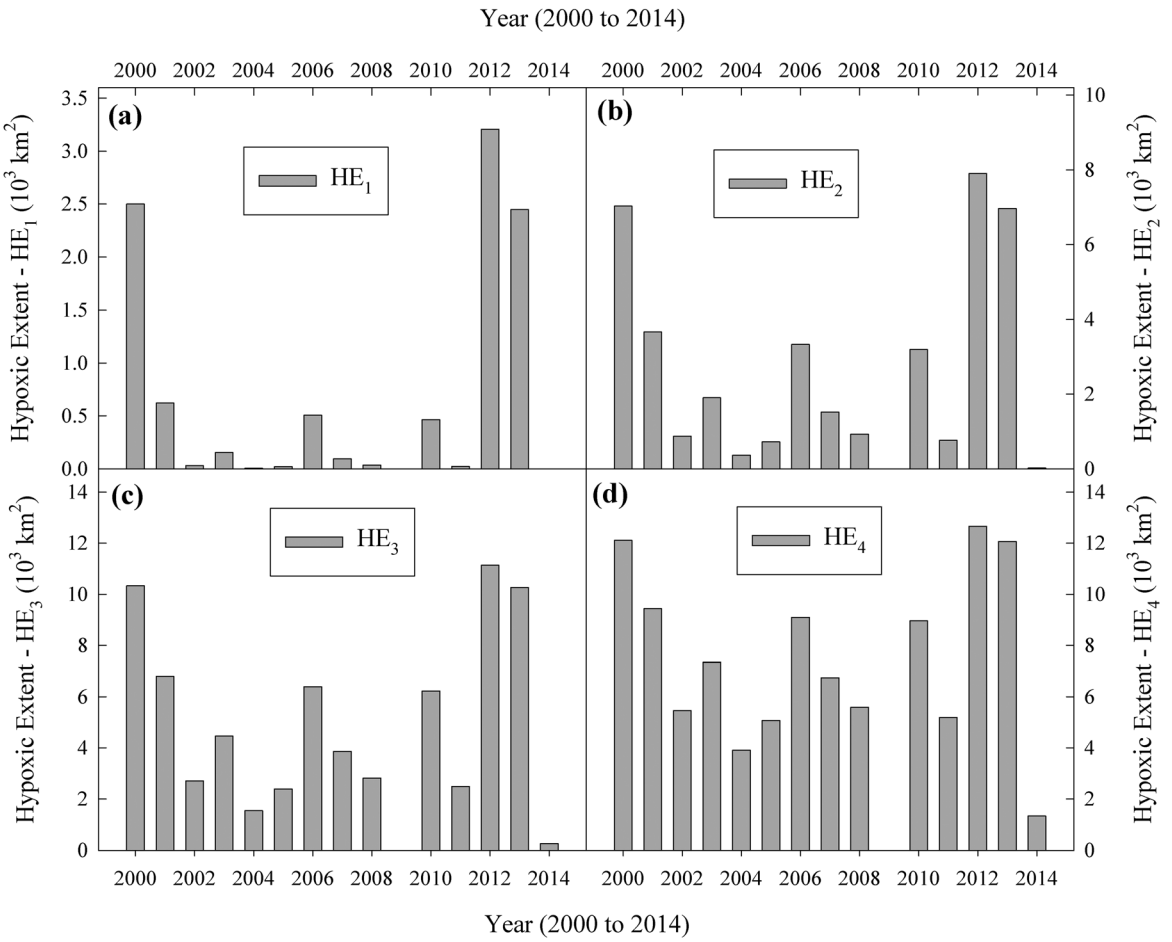

Figure 8. Estimated historical areal extents of central basin hypoxia for different threshold concentrations of DO < 1 (HE_1; a), < 2 (HE_2; b), < 3 (HE_3; c) and <4 mg L^{-1} (HE_4; d) for the past 15 years (2000–2014) based on the equations derived in this study (equations (2)–(5), Table 3) and observed DO concentrations during summer cruises (GLENDA data).

ultimate hypoxic area later in the summer and fall. Because our results are consistent with *Zhou et al.* [2013] through August and early September, we were able to extend the application later in the year using equations derived from our ELCD model output. We also developed equations to estimate the hypoxic extents of different DO thresholds (1, 2, 3 and 4 mg L^{-1}) as a function of mean bottom DO at the locations of Environment Canada index stations (Table 1), in addition to the USEPA index station, so that Environment Canada data can also be used in estimates of hypoxic extent.

While our results agreed well with those predicted by Zhou model for the data through approximately mid-September (Figure 5b), the divergence after that time (Figures 5c and 5a) coincides with the beginning of lake destratification and appears to be a result of wind stress beginning to dominate buoyancy forces, implying different underlying processes are in play.

During much of the warming season, buoyancy force is sufficient to overcome mixing and prevent oxygen flux from the epilimnion, favoring hypoxia formation and stability (supporting information Figures S2b). During this period, hypoxic area can be predicted well from knowledge of bathymetry and DO concentrations at index stations [e.g., *Zhou et al.*, 2013] because hypoxia development follows the bathymetry. However, when buoyancy forces decline in autumn (supporting information Figures S2b), hypoxia becomes more susceptible to strong wind events and associated mixing. At this time, the epilimnion deepens and the thermocline erodes as the lake continues to cool. As a result, Zhou's model may significantly underestimate hypoxic area at this time of year (Figure 5c). In mid-autumn, as the thermocline erodes, episodes of high winds (supporting information Figures S2) become more important for short-term fluctuations in hypoxic extent (Figure 5c; large variations and departures from 1:1 line), whereas the buoyancy is more important for longer-time scales (e.g., Figure 5b; points are getting closer to the 1:1 line).

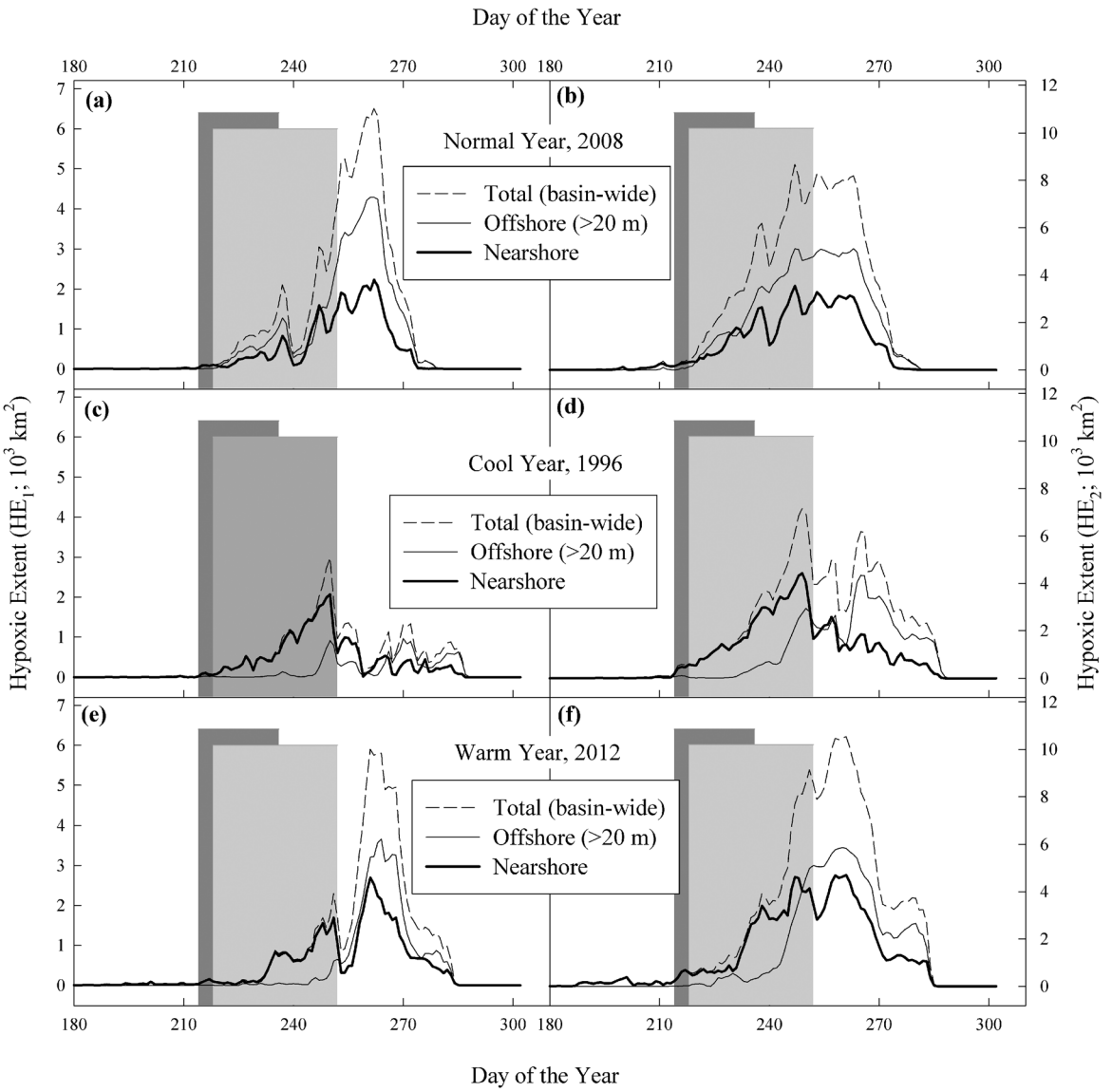

Figure 9. Simulated seasonal dynamics of HE_1 (a, c, e) and HE_2 (b, d, f) for basin-wide, nearshore and offshore zones in 2008 ("normal" year; a-b) and using meteorological conditions for 1996 (c–d) and 2012 (e–f) accounting for the meteorological conditions of the "cool" and "warm" years, respectively. The vertical light and dark grey bars indicate timing in days (mean ±SD) of all central basin DO monitoring cruises from 1987 to 2007 for all agencies (CLNPO, GLERL, and NWRI; $N = 75$) and some selected agencies (GLNPO and GLERL; $N = 26$), respectively, based on data provided in supporting information Table S1 in *Zhou et al*. [2013].

Our results also demonstrate that hypoxic extent usually reaches its maximum in September (Figure 9), whereas current monitoring programs typically end prior to that time. If maximum extent is a management metric [e.g., *IJC*, 2012], this suggests the need to add monitoring cruises through September, perhaps using models to schedule those later cruises adaptively. An alternative could be to deploy moorings with the DO sensors at 0.5–1 m above bottom at the locations of the USEPA index stations and use those observations and the equations in Table 3 to provide a more complete temporal characterization of seasonal hypoxia.

4.3. Different Thresholds

Because the impacts of low DO concentrations differs among processes and organisms [*Vaquer-Sunyer and Duarte*, 2008; *Farrell and Richards*, 2009; *Roberts et al*., 2009; *Vanderploeg et al*., 2009; supporting information Tables S1 and S2), we explored the dynamics of low oxygen areas defined by different thresholds. Our results (Figures 10a–10c) show that areas with DO less than 3 or 4 mg L^{-1} can occupy up to 75% and 85% of the central basin, respectively, and can last for as long as 3 months (e.g., Figure 10c). Therefore, the

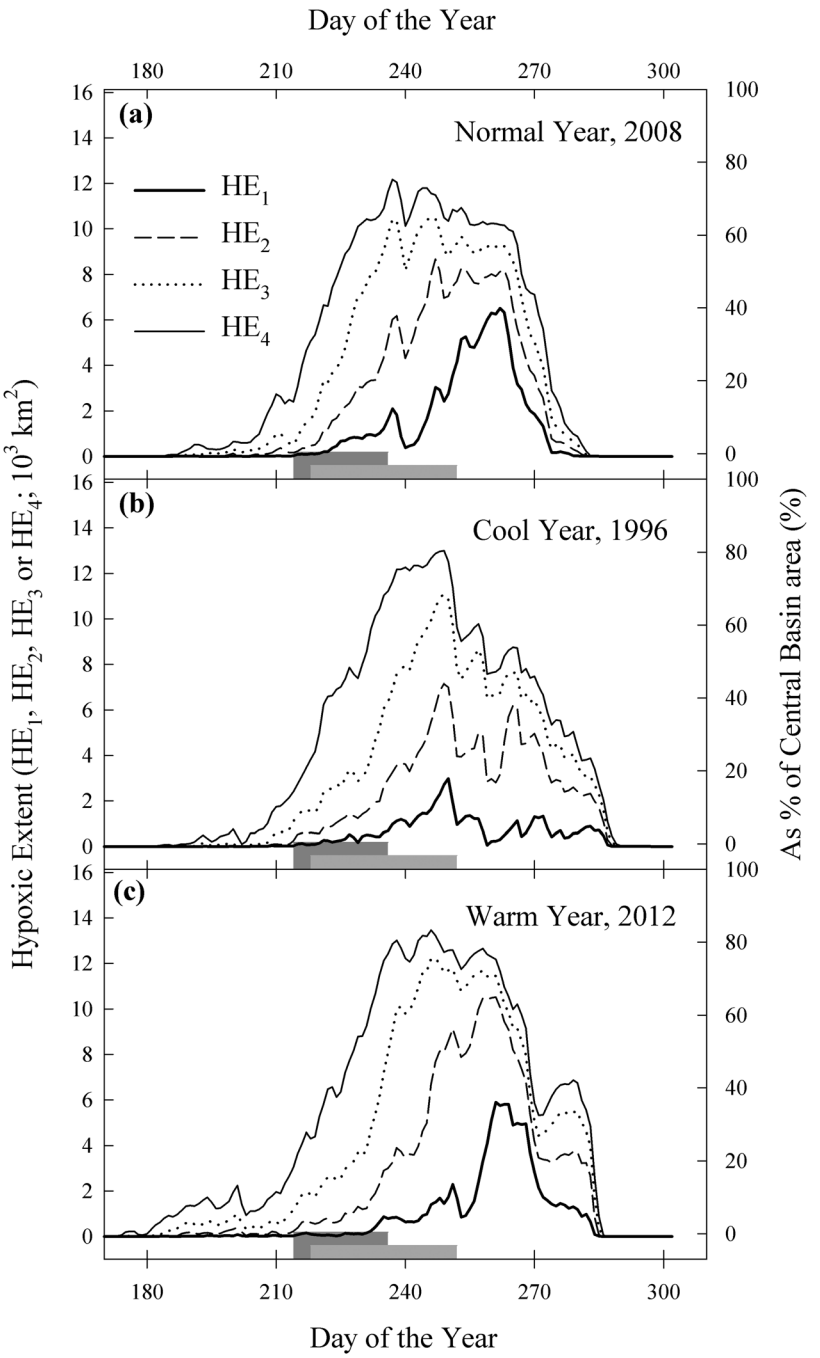

Figure 10. Simulated seasonal dynamics of the whole basin hypoxic extents HE_1, HE_2, HE_3, and HE_4 for (a) "normal" year, (b) "cool" year, and (c) "warm" year. See the legend of Figure 9 for the meanings of the vertical light and dark grey bars.

commonly used DO threshold of 2 mg L^{-1} may fail to reflect conditions where aquatic organisms experience hypoxia-induced responses. Because these thresholds are likely species and process specific, it could be possible to set different targets for Lake Erie, and use the equations in Table 3 and data from the USEPA or EC index stations to track associated conditions.

4.4. Spatial Dynamics

Despite a wide-spread belief that Lake Erie hypoxia starts at the deepest parts of the basin, our results present a first numerical demonstration that both hypoxia and anoxia start in the nearshore (Figure 9). This may

not be as clear during the "normal" year simulations (Figures 9a and 9b) but a closer examination shows that, even in that case, hypoxia appears first in the nearshore *albeit* for only a short time. Current monitoring programs are usually aimed at offshore conditions. However, the nearshore zone (defined here as depths $\leq$20 m), occupies a very significant portion of surface area of the central basin, and is the location of important habitat and drinking water intakes that have to be protected from hypoxic and anoxic waters. Our findings also demonstrated that nearshore hypoxia is significant and exists for extended periods (Figure 9), and that variations in climate, especially warmer meteorological conditions, may result in significant increases in hypoxia extent and duration in the nearshore (Figures 9b, 9d, and 9f). Therefore, it would be important to incorporate specific nearshore management criteria in future management and monitoring activities. In fact, the revised Great Lakes Water Quality Agreement [*IJC*, 2012] includes a new focus on the nearshore. It might be useful to employ the three-dimensional model like the one used here to identify critical areas in the nearshore for enhanced monitoring.

Acknowledgments
This work was supported in part by the National Science Foundation (NSF) under grant 1039043, the USEPA under contract EP-R5-11-07, Task Order 21, and the Graham Sustainability Institute of the University of Michigan. We are grateful to David Schwab for his advice and help with the interpolation of the meteorological data, as well as three anonymous reviewers. Data sets are available upon request by contacting the corresponding author (Serghei A. Bocaniov, bocaniov@umich.edu).

References

Arend, K. K., D. Beletsky, J. V. DePinto, S. A. Ludsin, J. J. Roberts, D. K. Rucinski, D. Scavia, D. J. Schwab, and T. O. Höök (2011), Seasonal and interannual effects of hypoxia on fish habitat quality in central Lake Erie, *Freshwater Biol.*, *56*(2), 366–383.

Beeton, A. M. (1963), Eutrophication of the St. Lawrence Great Lakes, *Limnol. Oceanogr.*, *10*, 240–254.

Beletsky, D., N. Hawley, and Y. R. Rao (2013), Modeling summer circulation and thermal structure of Lake Erie, *J. Geophys. Res. Oceans*, *118*, 6238–6252, doi:10.1002/2013JC008854.

Bocaniov, S. A., R. E. H. Smith, C. M. Spillman, M. R. Hipsey, and L. F. Leon (2014a), The nearshore shunt and the decline of the phytoplankton spring bloom in the Laurentian Great Lakes: Insights from a three-dimensional lake model, *Hydrobiologia*, *731*, 151–172.

Bocaniov, S. A., C. Ullmann, K. Rinke, K. G. Lamb, and B. Boehrer (2014b), Internal waves and mixing in a stratified reservoir: Insights from three-dimensional modeling, *Limnologica*, *49*, 52–67.

Bolsenga, S., and C. Herdendorf (Eds.) (1993), *Lake Erie and Lake St. Clair handbook*, Wayne State Univ. Press, Detroit, Mich.

Bridgeman, T. B., J. D Chaffin, and J. F. Filbrun (2013), A novel method for tracking western Lake Erie Microcystis blooms, 2002–2011, *J. Great Lakes Res.*, *39*(1), 83–89.

Brunt, D. (1927), The period of simple vertical oscillations in the atmosphere, *Q. J. R. Meteorol. Soc.*, *53*, 30–32.

Burns, N. M., D. C. Rockwell, P. E. Bertram, D. M. Dolan, and J. J. H. Ciborowski (2005), Trends in temperature, Secchi depth, and dissolved oxygen depletion rates in the central basin of Lake Erie, 1983–2002, *J. Great Lakes Res.*, *31*, 35–49.

Chesapeake Bay Watershed Agreement (2014), Chesapeake Bay Watershed Agreement, Chesapeake Bay Program, Annapolis, Md. [Available at <http://www.chesapeakebay.net/chesapeakebaywatershedagreement/page>, accessed 23 June 2015.]

Committee on Environment and Natural Resources (CENR) (2010), Scientific Assessment of Hypoxia in U.S. Coastal Waters, Interagency Working Group on Harmful Algal Blooms, Hypoxia, and Human Health of the Joint Subcommittee on Ocean Science and Technology, Washington, D. C. [Available at <http://www.whitehouse.gov/sites/default/files/microsites/ostp/hypoxia-report.pdf>, accessed 23 June 2015].

Committee on Environment and Natural Resources (CENR) (2000), An Integrated Assessment of Hypoxia in the Northern Gulf of Mexico. National Science and Technology Council Committee on Environment and Natural Resources, 58 pp., Washington, D. C. [Available at <http://oceanservice.noaa.gov/products/hypox_finalfront.pdf>, accessed 23 June 2015.]

Davison, W. (1993), Iron and manganese in lakes, *Earth Sci. Rev.*, *34*(2), 119–163.

DePinto, J. V., T. C Young, and L. M. McIlroy (1986), Great Lakes water quality improvement, *Environ. Sci. Technol.*, *20*(8), 752–759.

Diaz, R. J. (2001), Overview of hypoxia around the world, *J. Environ. Qual.*, *30*(2), 275–281.

Diaz, R. J., and R. Rosenberg (2008), Spreading dead zones and consequences for marine ecosystems, *Science*, *321*(5891), 926–929.

Dolan, D. M. (1993), Point source loadings of phosphorus to Lake Erie: 1986–1990, *J. Great Lakes Res.*, *19*(2), 212–223.

Dolan, D. M., and S. C. Chapra (2012), Great Lakes total phosphorus revisited: 1. Loading analysis and update (1994–2008), *J. Great Lakes Res.*, *38*(4), 730–740.

Farrell, A. P., and J. G. Richards (2009), Defining hypoxia: An integrative synthesis of the responses of fish to hypoxia, in *Hypoxia*, edited by J. G. Richards, A. P. Farrell, and C. J. Brauner, pp. 487–503, Academic, London, U. K., doi:10.1016/S1546-5098(08)00011-3.

Great Lakes Commission (2013), Annual Report of the Great Lakes Regional Water Use Database Representing 2011 Water Use Data, Issue 21, Ann Arbor, Mich. [Available at <http://projects.glc.org/waterusedata//pdf/wateruserpt2013.pdf>, accessed 15 July 2015.]

Hansson, M., L. Andersson, and P. Axe (2011), Areal extent and volume of anoxia and hypoxia in the Baltic Sea, 1960–2011, *SMHI Rep. Ser. Rep. Oceanogr.*, *42*, Swedish Meteorological and Hydrological Institute (SMHI), Norrköping, Sweden.

Hawley, N., T. H. Johengen, Y. R. Rao, S. A. Ruberg, D. Beletsky, S. A. Ludsin, B. J. Eadie, D. J. Schwab, T. E. Croley, and S. B. Brandt (2006), Lake Erie hypoxia prompts Canada-U.S. study, *Eos Trans. AGU*, *87*(32), 313–319, doi:10.1029/2006EO320001.

Helsinki Commission (2007), HELCOM Baltic Sea Action Plan, Baltic Mar. Environ. Prot. Comm., 102 pp., Helsinki, Finland. [Available at <http://www.helcom.fi/baltic-sea-action-plan>, accessed 15 June 2015.]

Hipsey, M. R. (2008), *The CWR Computational Aquatic Ecosystem Dynamics Model CAEDYM. User Manual*, Cent. for Water Res., Univ. of West. Aust., Perth, Australia.

Hodges, B., and C. Dallimore (2006), *Estuary, Lake and Coastal Ocean Model: ELCOM. Science Manual*. Cent. of Water Res., Univ. of West. Aust., Perth, Australia.

Hodges, B., J. Imberger, A. Saggio, and K. Winters (2000), Modeling basin-scale internal waves in a stratified lake, *Limnol. Oceanogr.*, *45*, 1603–1620.

Howarth, R., F. Chan, D. J. Conley, J. Garnier, S. C. Doney, R. Marino, and G. Billen (2011), Coupled biogeochemical cycles: Eutrophication and hypoxia in temperate estuaries and coastal marine ecosystems, *Front. Ecol. Environ.*, *9*, 18–26.

Huang, A., Y. R. Rao, Y. Lu, and J. Zhao (2010), Hydrodynamic modeling of Lake Ontario: An intercomparison of three models, *J. Geophys. Res.*, *115*, C12076, doi:10.1029/2010JC006269.

International Commission for the Protection of the Danube River (2006), Danube Pollution Reduction Programme. [Available at <http://www.icpdr.org/icpdr-pages/dprp.htm>, accessed 29 June 2015.]

International Commission for the Protection of the Danube River (2009), Danube River Basin District Management Plan. [Available at <http://www.icpdr.org/icpdr-files/15091>, accessed 15 July 2015.]
Idso, S. B. (1973), On the concept of lake stability, *Limnol. Oceanogr.*, *18*, 681–683.
Idso, S. B., and R. D. Jackson (1969), Thermal radiation from the atmosphere, *J. Geophys. Res.*, *74*, 5397–5403.
International Joint Commission (IJC) (2012), Great Lakes Water Quality Agreement 2012. Protocol Amending the Agreement between Canada and the United States of America on Great Lakes Water Quality, Windsor, Ontario, Canada, 7 Sept. 2012.
Imberger, J. (1985), The diurnal mixed layer, *Limnol. Oceanogr.*, *30*(4), 737–770.
Kraus, R. T., C. T Knight, T. M. Farmer, A. M. Gorman, P. D. Collingsworth, G. J. Warren, P. M. Kocovsky, and J. D. Conroy (2015), Dynamic hypoxic zones in Lake Erie compress fish habitat, altering vulnerability to fishing gears, *Can. J. Fish. Aquat. Sci.*, *72*(6), 797–806, doi: 10.1139/cjfas-2014-0517.
Leon, L. F., R. E. H. Smith, M. R. Hipsey, S. A. Bocaniov, S. N. Higgins, R. E. Hecky, J. P. Antenucci, J. A. Imberger, and S. J. Guildford (2011), Application of a 3D hydrodynamic-biological model for seasonal and spatial dynamics of water quality and phytoplankton in Lake Erie, *J. Great. Lakes. Res.*, *37*, 41–53.
Liu, W., S. A. Bocaniov, K. G. Lamb, and R. E. H. Smith (2014), Three dimensional modeling of the effects of changes in meteorological forcing on the thermal structure of Lake Erie, *J. Great Lakes Res.*, *40*, 827–840.
Michalak, A. M., et al. (2013), Record-setting algal bloom in Lake Erie caused by agricultural and meteorological trends consistent with expected future conditions, *Proc. Natl. Acad. Sci. U. S. A.*, *110*(16), 6448–6452.
Mississippi River/Gulf of Mexico Watershed Nutrient Task Force (MR/GOM) (2001), Action plan for reducing, mitigating, and controlling hypoxia in the northern Gulf of Mexico, Off. of Wetlands, Oceans, and Watersheds, U.S. Environ. Prot. Agency, Washington, D. C.
Mississippi River/Gulf of Mexico Watershed Nutrient Task Force (MR/GOM) (2008), Gulf hypoxia action plan, Off. of Wetlands, Oceans, and Watersheds, U.S. Environ. Protect. Agency, Washington, D. C.
Obenour, D., D. Scavia, N. R. Rabalais, E. R. Turner, and A. Michalak (2013), A retrospective analysis of mid-summer hypoxic area and volume in the northern Gulf of Mexico, 1985-2011, *Environ. Sci. Technol.*, *47*, 9808−9815.
Obenour, D. R., A. M. Michalak, and D. Scavia (2015), Assessing biophysical controls on Gulf of Mexico hypoxia through probabilistic modeling, *Ecol. Appl.*, *25*(2), 492–505.
Parkinson, C. L., and W. M. Washington (1979), A large-scale numerical model of sea ice, *J. Geophys. Res.*, *84*, 311–337.
Rabalais, N. N., R. E. Turner, and W. J. Wiseman Jr. (2002), Gulf of Mexico hypoxia, AKA'' The dead zone'', *Annu. Rev. Ecol. Syst.*, *33*, 235–263.
Rabalais, N. N., R. E. Turner, B. S. Gupta, D. F. Boesch, P. Chapman, and M. C. Murrell (2007), Hypoxia in the northern Gulf of Mexico: Does the science support the plan to reduce, mitigate, and control hypoxia?, *Estuarine Coasts*, *30*(5), 753–772.
Rao, Y. R., T. Howell, S. B. Watson, and S. Abernethy (2014), On hypoxia and fish kills along the north shore of Lake Erie, *J. Great Lakes Res.*, *40*, 187–191.
R Core Team (2014*), R: A Language and Environment for Statistical Computing*, R Found. for Stat. Comput., Vienna, Austria. [Available at <http://www.R-project.org/>, accessed 15 June 2015.]
Read, J. S., D. P. Hamilton, I. D. Jones, K. Muraoka, L. A. Winslow, R. Kroiss, C. H. Wu, and E. Gaiser (2011), Derivation of lake mixing and stratification indices from high-resolution lake buoy data, *Environ. Modell. Software*, *26*(11), 1325–1336.
Renaud, M. L. (1986), Hypoxia in Louisiana coastal waters during 1983: Implications for fisheries, *Fish. B-NOAA*, *84*, 19–26.
Roberts, J. J., T. O. Höök, S. A. Ludsin, S. A. Pothoven, H. A. Vanderploeg, and S. B. Brandt (2009), Effects of hypolimnetic hypoxia on foraging and distributions of Lake Erie yellow perch, *J. Exp. Mar. Biol. Ecol.*, *381*, S132–S142.
Rodgers, G. K., and D. V. Anderson (1961), A preliminary study of the energy budget of Lake Ontario, *J. Fish. Res. Board Can.*, *18*(4), 617–636.
Ruberg, S. A., E. Guasp, N. Hawley, R. W. Muzzi, S. B. Brandt, H. A. Vanderploeg, J. C. Lane, T. Miller, and S. A. Constant (2008), Societal benefits of the real-time coastal observation network (ReCON): Implications for municipal drinking water quality, *Mar. Technol. Soc. J.*, *42*(3), 103–109.
Rucinski, D. K., J. V. DePinto, D. Scavia, and D. Beletsky (2014), Modeling Lake Erie's hypoxia response to nutrient loads and physical variability, *J. Great Lakes Res.*, *40*, 151–161.
Sambridge, M., J. Braun, and H. McQueen (1995), Geophysical parametrization and interpolation of irregular data using natural neighbours, *Geophys. J. Int.*, *122*, 837–857.
Scavia, D., and J. V. DePinto (2015), Great Lakes Water Quality Agreement Nutrient Annex Objectives and Targets Task Team Ensemble Modeling Report, 229 pp., University of Michigan, Ann Arbor, Mich. [Available at <http://tinyurl.com/ng6d3tn>, accessed 10 Aug. 2015.]
Scavia, D., et al.(2014), Assessing and addressing the re-eutrophication of Lake Erie: Central basin hypoxia. *J. Great Lakes Res.*, *40*(2), 226–246.
Schertzer, W. M., J. H Saylor, F. M. Boyce, D. G. Robertson, and F. Rosa (1987), Seasonal thermal cycle of Lake Erie, *J. Great Lakes Res.*, *13*(4), 468–486.
Schmidt, W. (1928), Über die Temperatur-und Stabilitätsverhältnisse von Seen, *Geograf. Ann.*, *10*, 145–177.
Schwab, D. J., and J. A. Morton (1984), Estimation of overlake wind speed from overland wind speed: A comparison of three methods, *J. Great Lakes Res.*, *10*(1), 68–72, doi:10.1016/S0380-1330(84)71808-9.
Sly, L. I., M. C. Hodgkinson, and V. Arunpairojana (1990), Deposition of manganese in a drinking water distribution system, *Appl. Environ. Microb.*, *56*(3), 628–639.
U.S. Environmental Protection Agency (2010), Chesapeake Bay total maximum daily load for nitrogen, phosphorus, and sediment, U.S. Environ. Protect. Agency, Chesapeake Bay Program Off., Annapolis, Md. [Available at <http://www.epa.gov/reg3wapd/tmdl/ChesapeakeBay/tmdlexec.html>, accessed 15 June 2015.]
Väisälä, V. (1925), Über die Wirkung der Windschwankungen auf die Pilotbeobachtungen, *Soc. Sci. Fenn. Commentat. Phys. Math.*, *2*(19), 19–37.
Vanderploeg, H. A., S. A. Ludsin, S. A. Ruberg, T. O. Höök, S. A. Pothoven, S. B. Brandt, G. A. Lang, J. R. Liebig, and J. F. Cavaletto (2009), Hypoxia affects spatial distributions and overlap of pelagic fish, zooplankton, and phytoplankton in Lake Erie, *J. Exp. Mar. Biol. Ecol.*, *381*, S92–S107.
Vaquer-Sunyer, R., and C. M. Duarte (2008), Thresholds of hypoxia for marine biodiversity, *Proc. Natl. Acad. Sci. U. S. A.*, *105*(40), 15,452–15,457.
Zhou, Y., D. R. Obenour, D. Scavia, T. H. Johengen, and A. M. Michalak (2013), Spatial and temporal trends in Lake Erie hypoxia, 1987–2007, *Environ. Sci. Technol.*, *47*, 899–905, doi:10.1021/es303401b.
Zhou, Y., D. Scavia, and A. M. Michalak (2014), Nutrient loading and meteorological conditions explain interannual variability of hypoxia in the Chesapeake Bay, *Limnol. Oceanogr.*, *59*, 373–374, doi:10.4319/lo.2014.59.2.0373.
Zhou, Y., A. M. Michalak, D. Beletsky, Y. R. Rao, and R. P. Richards (2015), Record-breaking Lake Erie hypoxia during 2012 drought, *Environ. Sci. Technol.*, *49*(2), 800–807, doi:10.1021/es503981n.